ISEV

Targeting extracellular vesicle delivery to the lungs by microgel encapsulation

Nicholas D. Cober[1,2] | **Katelynn Rowe**[1] | **Yupu Deng**[1] | **Ainara Benavente-Babace**[3] | **David W. Courtman**[1] | **Michel Godin**[3] | **Duncan J. Stewart**[1,2]

[1]Sinclair Centre for Regenerative Medicine, Ottawa Hospital Research Institute, Ottawa, Ontario, Canada

[2]Faculty of Medicine, Department of Cellular and Molecular Medicine, University of Ottawa, Ottawa, Ontario, Canada

[3]Faculty of Science, Department of Physics, University of Ottawa, Ottawa, Ontario, Canada

Correspondence
Duncan J. Stewart, The Ottawa Hospital, Ottawa Hospital Research Institute, The Evelyne & Rowell Laishley Chair and Professor, Department of Medicine, University of Ottawa, 501 Smyth Road, Box/C.P. 511, Ottawa, Ontario, K1H 8L6, Canada.
Email: djstewart@ohri.ca

Funding information
Canadian Institutes of Health Research, Grant/Award Number: FDN–143291

Abstract

Extracellular vesicles (EVs) secreted by stem and progenitor cells have significant potential as cell-free 'cellular' therapeutics. Yet, small EVs (<200 nm) are rapidly cleared after systemic administration, mainly by the liver, presenting challenges targeting EVs to a specific organ or tissue. Microencapsulation using natural nanoporous hydrogels (microgels) has been shown to enhance engraftment and increase the survival of transplanted cells. We sought to encapsulate EVs within microgels to target their delivery to the lung by virtue of their size-based retention within the pulmonary microcirculation. Mesenchymal stromal cell (MSC) derived EVs were labelled with the lipophilic dye (DiR) and encapsulated within agarose-gelatin microgels. Endothelial cells and bone marrow derived macrophages were able to take up EVs encapsulated in microgels in vitro, but less efficiently than the uptake of free EVs. Following intrajugular administration, microgel encapsulated EVs were selectively retained within the lungs for 72h, while free EVs were rapidly cleared by the liver. Furthermore, microgel-loaded EVs demonstrated greater uptake by lung cells, in particular CD45^{+} immune cells, as assessed by flow cytometry compared to free EVs. Microencapsulation of EVs may be a novel tool for enhancing the targeted delivery of EVs for future therapeutic applications.

KEYWORDS
biodistribution, biomaterials, extracellular vesicles, microencapsulation, pulmonary circulation

1 | INTRODUCTION

There is increasing evidence that extracellular vesicles (EVs) play an essential role in cell-to-cell communication (Colombo et al., 2014). EVs are nano-sized membrane bound particles loaded with proteins, mRNAs and miRNAs from their host cell which provide important signalling cues to their recipient cell (Colombo et al., 2014). EVs can be categorised based on their size; small EVs are <150 nm in size and likely contain the exosome fraction of endosomal origin, whereas EVs between 150 and 1000 nm contain primarily microvesicles (Théry et al., 2018). Mesenchymal stromal cells (MSCs) represent a multi-faceted therapeutic cell with important angiogenic and immunomodulatory potential and have been reported to have therapeutic effects in a number of models of cardiovascular disease (Willis et al., 2018). The actions of MSCs are thought to be mediated largely by paracrine mechanisms, in particular related to the release of therapeutic EVs (Cruz & Rocco, 2017). Therefore, there is considerable interest in developing MSC derived EVs, particularly small EVs, as a cell-free 'cellular' therapeutic product (Cruz & Rocco, 2017). In fact, MSC-EVs have been studied as a therapy for a variety of cardiovascular diseases including pulmonary arterial hypertension

(PAH) (Bian et al., 2014; de Mendonça et al., 2017; Klinger et al., 2019), acute myocardial infarction (Bian et al., 2014; Wang et al., 2017), acute lung injury (Wang et al., 2020) and broncho-pulmonary dysplasia (Porzionato et al., 2021).

EVs have a number of potential advantages over intact cells. EVs have the potential to mirror the benefits of cell-based therapies without some of the risks associated with delivery of intact cells, including tumorigenicity, immunoreactivity, product shelf life and viability (Tieu et al., 2020). As MSC-EVs are cell by-products they are unable to replicate and cannot directly form tumours. Furthermore, the transplantation of allogenic cells presents a risk of immunoreactivity from foreign antigens, whereas EVs derived from MSCs generally lack components of the major histocompatibility complex (Kou et al., 2022). Finally, unlike intact cells where efficacy is dependent on cell viability that can be lost during storage (Wilson et al., 2015), EVs possess good long-term stability at $-80°C$ (Yuana et al., 2015) and do not have post thaw viability requirements that may hinder their use.

However, unlike intact cells which can be used to target the lung through size-based filtration in the distal lung arteriolar bed, small EVs, in the nanometre range, would not be expected to lodge in the precapillary arteriolar bed and are rapidly cleared from the circulation by the liver and spleen (Lai et al., 2014; Wiklander et al., 2015), limiting their therapeutic potential. Indeed, Gupta et al. have shown in a pharmacokinetic study that EVs have a very short half-life in vivo and are cleared from the blood within minutes of delivery (Gupta et al., 2020). Furthermore, biodistribution may be impacted by cell origin; while EVs from many cell types largely accumulate in the liver and spleen (Wiklander et al., 2015), EVs derived from breast cancer cells may preferentially target the lung (Wen et al., 2016), as well as by modifications, such as glycosylation (Royo et al., 2019), or genetic modification (Wen et al., 2021).

Biomaterials are commonly used to create cell compatible microenvironments, promoting cell viability and facilitating transplantation (Thomas et al., 2018), and can be engineered to target distribution to a particular organ. Microencapsulation can enhance local organ retention of intact cells (Karoubi et al., 2009) and has been shown to promote therapeutic outcomes in experimental models of acute myocardial infarction (Kanda et al., 2018). More recently, bulk EV encapsulation has been used to create large regenerative tissue patches for cardiac repair (Lv et al., 2019). Despite relatively poor lung uptake after intravascular delivery (Wiklander et al., 2015), EVs have been shown to be effective in the treatment of preclinical models of PAH (Xu et al., 2022). Therefore, the objective of this study was to determine whether microencapsulation of EVs within nanoporous hydrogels (microgels) would increase lung targeting in the monocrotaline (MCT) preclinical model of (PAH). We hypothesised that microencapsulation of EVs would enhance local EV retention within the diseased lung, facilitating increased cellular uptake. We now report markedly enhanced retention of EV-loaded microgels within the lungs as compared to free EVs, with enhanced local cellular uptake, supporting the use of microencapsulation as a novel strategy to efficiently target EVs to the lung.

2 | METHODS

2.1 | MSC culture and EV isolation

Sprague Dawley rat bone marrow MSCs were isolated from rat bone marrow as previously described by Song et al. (2014) or acquired from Cyagen (Cyagen Bioscience, Santa Clara, CA). Isolated rat bone marrow MSCs were cultured in alpha MEM (ThermoFisher Scientific, Burlington ON, Canada) with 10% fetal bovine serum (ThermoFisher Scientific, Burlington ON, Canada) and 1% penicillin/streptomycin (Life Technologies, Carlsbad, CA), Cyagen sourced MSCs were cultured in StemXVivo mesenchymal stem cell expansion media (R&D systems, Toronto, ON, Canada) inside tissue culture incubators at 37°C with 5% CO_2, passaging as necessary.

2.2 | EV isolation and labelling

MSCs between passages 3 and 5 were used for EV isolations. For EV isolation, MSCs were cultured to 80%–90% confluency, washed 2x with PBS and changed to serum free alpha-MEM (Invitrogen, Waltham, MA) with 1% penicillin-streptomycin for 24 h collection period. After 24 h, MSC-conditioned media was collected and purified using sequential ultracentrifugation and tangential flow filtration (TFF) (KrosFlow KR2i, Repligen, Waltham, MA). Since TFF coupled with ultra-centrifugation may lead to co-precipitation of protein aggregates, we were careful to apply consistent production processes in these experiments to minimise any confounding effects from uptake of protein aggregates. In brief, conditioned media (CM) was spun at $2500 \times g$ for 10 min at 4°C, the supernatant was then spun at $20,000 \times g$ for 20 min at 4°C. The resulting conditioned media was processed by TFF to remove small protein and particles with a 500,000 MWCO MidGee hoop ultrafiltration cartridge (GE Lifesciences, Vancouver, BC, Canada). Diafiltration was performed with sterile filtered PBS and concentrated sample was collected. To further purify small EVs, conditioned media was spun at $100,000 \times g$ for 30 min at 4°C and pellets were resuspended in sterile PBS. For DiR (ThermoFisher Scientific, Burlington, ON, Canada) and DiD (ThermoFisher Scientific, Burlington, ON, Canada) labelling, concentrated EVs from the TFF were stained with DiR or DiD at 0.5 μg/mL for 15 min then spun at $100,000 \times g$ for 30 min at 4°C to wash unbound dye and pellets were resuspended in PBS. For pkh26 (Sigma Aldrich, Oakville, ON, Canada) labelling,

concentrated EV fraction following TFF was spun at $100,000 \times g$ for 30 min at 4°C, and pellets were resuspended in dilutant C. pkh26 (0.002 mM; Sigma Aldrich, Oakville, ON, Canada) was added for 15 min following which sample was spun at $100,000 \times g$ for 30 min at 4°C to concentrate and wash the EV fraction. Labelled EVs were resuspended in PBS, aliquoted and stored at −80°C until use.

2.3 | EV characterisation

MSC-derived small EVs were characterised for protein concentration using the bicinchoninic acid (BCA) assay (Sigma Aldrich, Oakville, ON, Canada). Nanoparticle tracking analysis was performed using ZetaView (Particle Metrix, Mebane, NC) to determine particle number and size distribution. Western blot was performed to confirm presence of canonical EV protein markers CD63, CD9, TSG101, or negative selection marker GM-130. Samples were lysed in 1x RIPA buffer (Millipore, CA) + Halt protease inhibitors (ThermoFisher Scientific, Burlington, ON, Canada) with sonication and vortexing for protein quantification, as above. Loading buffer was added and samples were heated at 70°C for 10 min. Samples (10–15 μg protein/lane) were run by electrophoresis on pre-cast SDS–PAGE Stain Free Gels (Bio-Rad, Hercules, CA). Separated proteins were transferred to low fluorescence PVDF membranes using the TransBlot Turbo (Bio-Rad, Hercules, CA), and blocked in TBS-T (TBS with 0.1% Tween 20) with 5% non-fat dry milk for 1 h at room temperature. Membranes were washed 5× times with TBS-T and stained overnight at 4°C with gentle agitation with primary antibodies: mouse anti-rat CD63 (1:200 dilution, BD Biosciences, Mississauga, ON, Canada), rabbit anti-rat CD9 (1:500 dilution, ThermoFisher Scientific, Burlington, ON, Canada), rabbit anti-rat TSG101 (1:500 dilution, ThermoFisher Scientific, Burlington, ON, Canada), or rabbit anti-mouse GM-130 (1:500 dilution, ThermoFisher Scientific, Burlington, ON, Canada). After washing membranes 5x in TBS-T membranes were incubated with appropriate horseradish peroxidase (HRP)-conjugated secondary antibodies (1:5000, Jackson ImmunoResearch West Grove, PA) for 1 h at room temperature. Clarity Western ECL (Bio-Rad, Hercules, CA) was used to detect HRP signal imaging with ChemiDoc MP imaging system (Bio-Rad Hercules, CA). Images were analysed with Image Lab v6 (Bio-Rad, Hercules, CA). Data shown in Figure S1.

2.4 | HUVEC uptake experiments

Human umbilical vein endothelial cells (HUVEC) were cultured in endothelial cell (EC) growth media with 5% FBS, 1% pen/strep and supplements (ScienCell, Carlsbad, CA), in a tissue culture incubator at 37°C with 5% CO_2, passaging as needed. HUVEC between passages 4 and 6 were used for experiments. HUVEC were seeded at 100,000 cells per well in a 6-well plate (Corning, Corning, NY), after 24 h DiR or DiD labelled free EVs were added at 1 μg or 3 μg of EV protein. After 24 h of uptake, cells were washed with PBS, lifted with trypLE (Life Technologies, Carlsbad, CA), and resuspended in **PEB**: **P**BS + 2 mM **E**DTA (ThermoFisher Scientific, Burlington, ON, Canada) + 0.5% **b**ovine serum albumin (BSA, Wisent Bioproducts, Saint-Jean-Baptiste, QC, Canada). Cells were counted, washed and resuspended in staining buffer containing: 1:100 dilution V450 mouse anti-human CD31 (BD Biosciences, Mississauga, ON, Canada), 1:10 dilution PE mouse anti-human CD34 (BD Biosciences, Mississauga, ON, Canada), for 30 min at 4°C in the dark. Appropriate unstained, fluorescent minus one (FMOs) and compensation controls were prepared. Following staining cells were washed with PEB and loaded into 5 mL flow tube (Corning, Corning, NY) for flow analysis on the Attune NXT (ThermoFisher Scientific, Burlington, ON, Canada), or the AMNIS ImageStream X (Luminex, Austin, TX) for intracellular visualisation. Subsequent analysis was performed in FlowJo version 10 (FlowJo LLC, Ashland, OR).

2.5 | Bone marrow derived macrophage isolation, characterisation and uptake

Rat bone marrow derived macrophages were derived, as adapted from Souza-Moreira et al. (2019). Rat bone marrow was isolated, mononuclear cells were counted and frozen in 90% heat inactivated (HI) FBS (ThermoFisher Scientific, Burlington, ON, Canada) + 10% DMSO (Sigma Aldrich, Oakville, ON, Canada). Rat bone marrow mononuclear cells were thawed and cultured at 4–6 million in a 10 cm dish (Falcon) using differentiation media containing: DMEM (ThermoFisher Scientific, Burlington, ON, Canada), 20% HI FBS, 1% Pen/strep, 1% Glutamax (ThermoFisher Scientific, Burlington, ON, Canada) and 20 ng/mL macrophage colony stimulating factor (MCSF, Sigma Aldrich, Oakville, ON, Canada) in a tissue culture incubator at 37°C, 5% CO_2. Additional media was added after 3–4 days. After 6–7 days macrophages were lifted using cold PBS and scraping then counted. Bone marrow derived macrophages were plated at 1 million per well, in a 6-well plate in DMEM + 10% HI FBS, 1% Pen-strep, 1% glutamax with or without LPS (50 ng/mL, Sigma Aldrich, Oakville, ON, Canada) + interferon gamma (IFNγ, 5 ng/mL PeproTech Inc., Cranberry, NJ) or interleukin 4 (IL4, 10 ng/mL, PeproTech Inc., Cranberry, NJ) stimulation. Macrophages were characterised for presence and absence of canonical markers using flow cytometry PE-Cy5 mouse anti-rat CD45 (BD Biosciences, Mississauga, ON, Canada), BV786 mouse anti-rat CD11b/c (BD Biosciences, Mississauga, ON, Canada) and PE mouse anti-rat CD34

(Novus Biologicals, Littleton, CO) (Figure S2). For uptake experiments macrophages were cultured, lifted and plated for 24 h of stimulation with or without LPS+IFNγ. Subsequently, macrophages were washed with PBS, and fresh media was added with or without IL4, and DiR labelled EVs at 1 μg of EV protein. After 24 h macrophages were lifted, washed, counted and stained. Staining was performed with 1:200 dilution eFluor 450 mouse anti-rat CD45 (eBioscience, San Diego, CA), and FITC mouse anti-rat CD86 (eBioscience, San Diego, CA), for 30 min at 4°C in the dark. Following which cells were washed and analysed by flow cytometry as previously described.

2.6 | Microfluidic EV encapsulation

EVs were encapsulated using a novel microfluidic device designed for cell and small particle encapsulation, in a similar manner as described for cell encapsulation (Benavente-Babace et al., 2019; Kanda et al., 2020). A known quantity of EV protein (10–20 μg) was mixed with 1% ultra-low gelling temperature agarose (Sigma Aldrich, Oakville, ON, Canada), 1% gelatin (Sigma Aldrich, Oakville, ON, Canada) and kept at 37°C during encapsulation. Following microfluidic encapsulation, microgels were kept at 4°C to ensure complete gelation, and 3x PBS washes with $1000 \times g$ for 5 min centrifugation spins to remove the residual oil. Microgels were counted using the hemocytometer and used for experiments based on initial EV protein incorporated into the total batch of microgels. Microgels were stored at 4°C for up to 24 h prior to in vivo injection. For fluorescent visualisation gelatin labelled with Oregon green 488 (ThermoFisher Scientific, Burlington, ON, Canada) was added to capsules at a diluted concentration (0.5%). Fluorescently labelled EV-loaded and empty microgels were visualised with both a Zeiss M2 imager epi-fluorescent and a Zeiss LSM900 confocal microscope.

2.7 | MCT model of PAH and biodistribution

All animal experiments were approved by the University of Ottawa Animal Care Committee. As previously described by Zhao et al. (2005), male Sprague Dawley (SD) rats (200–250 g) were injected with monocrotaline (MCT) (60 mg/kg, Sigma Aldrich, Oakville, ON, Canada) by intra peritoneal (i.p.) injection 7 days before EV injections. For EV injections, animals were anaesthetised by isoflurane inhalation for jugular vein cut down and cannulation. After wound closure, topical bupivacaine was applied, and administered twice daily for 1 day following surgery. Buprenorphine (s.c. 0.03 mg/kg, Ceva Santé Animale, Libourne, France) was also administered 1 h prior to surgery for pain management. Treatments were delivered by intra jugular vein (i.j.) injection using PBS (ThermoFisher Scientific, Burlington, ON, Canada) vehicle. For biodistribution experiments of DiR labelled free or encapsulated EVs (20 μg protein content) were tracked at 4 h, 24 h and 72 h post injection by ex vivo imaging with the IVIS spectrum (Perkin Elmer, Waltham, MA) at the University of Ottawa Preclinical Imaging Core (RRID:SCR_021832). Animals were euthanised, organs (lungs, liver, spleen, kidney and heart) were isolated and fluorescent images were acquired. Region of interest selection for average radiant efficiency were selected using Living Image Software v 3.2 (Perkin Elmer, Waltham, MA) intensity and fluorescent background was subtracted using vehicle controls.

2.8 | Lung digestion and flow analysis

As described, EVs or microgel-EVs were injected 7 days following MCT injection. Lung digestion was performed as previously described (Godoy et al., 2021; Hurskainen et al., 2021). Twenty-four hours post injection animals were euthanised, and lungs were flushed with PBS perfusion through the right heart. Lungs were extracted, manually diced and placed in OCTO-Macs dissociation tubes (Miltenyi Biotec, Bergisch Gladbach, Germany) with digestion buffer [collagenase type 1 (Worthington Biochem., Lakewood, NJ) neutral protease (Worthington Biochem., Lakewood, NJ), and DNAase I (Sigma Aldrich, Oakville, ON, Canada) in Hank's Balanced Salt Solution (HBSS, ThermoFisher Scientific, Burlington, ON, Canada)]. Dissociation was performed using OCTOmacs dissociator (Miltenyi Biotec, Bergisch Gladbach, Germany). Following which, digested lungs were filtered through 70 μm filters (Corning, Corning, NY) and washed with PEB. Red blood cell lysis was performed with 1x RBC lysis buffer (eBioscience, San Diego, CA) for 3 min at room temperature, followed by washing with PEB. Cells were counted in PEB and ~1 million cells were taken for staining and appropriate controls. Cells were stained with first Live/Dead Fixable yellow (ThermoFisher Scientific, Burlington, ON, Canada), and then 1:200 dilution of Alexa Fluor 488 mouse anti-rat CD45 (BioLegend, San Diego, CA), PE mouse anti-rat CD31 (BD biosciences, Mississauga, ON, Canada) for 30 min at 4°C in the dark. Cells were washed with PEB, mixed with CountBright Plus absolute counting beads (ThermoFisher Scientific, Burlington, ON, Canada), and analysed by flow cytometry on the Attune Nxt (ThermoFisher Scientific, Burlington, ON, Canada), with subsequent analysis performed in FlowJo v10 (FlowJo LLC, Ashland, OR). Gating strategy shown in Figure S3.

2.9 | Statistical analysis

All data are presented as means $\pm$ SEM. Differences between groups were analysed by one-way with Tukey's post-hoc test for multiple comparisons or two-way analysis of variance (ANOVA) with Sidak's post-hoc test for multiple comparisons. An adjusted p-value of $p < 0.05$ was considered significant. All statistical analysis was performed with Graph Pad Prism 8.0 (Graph Pad, San Diego, CA).

3 | RESULTS

3.1 | Differential uptake of EVs by cell type

Small EVs are known to play a role in cellular communication in part mediated by uptake by other cells. Small MSC-derived EVs labelled with the near infrared lipophilic dye DiR were incubated with HUVEC or bone marrow-derived macrophages in vitro. Less than a third of HUVECs ($29 \pm 2\%$) were observed to take up DiR labelled EVs over 24 h at 1 μg of protein (Figure 1a–c), although this increased with higher protein concentration ($62 \pm 3\%$ at 3 μg). Visualisation with the AMNIS image stream (Figure 1b) and subsequently confocal imaging (Figure S4) demonstrated the labelled EVs were internalised, not only bound to the cell surface. Compared to HUVECs, a greater proportion of untreated macrophages (MØ) were readily able to take up EVs ($75 \pm 4\%$ at 1 μg) (Figure 1d,e) which had no discernible effect on MØ morphology (Figure S5). Pretreatment with IL4 to induce a M2 alternative activation state, but not LPS+IFNγ which promotes an M1 phenotype, significantly reduced the uptake of MSC EVs ($p = 0.03$) (Figure 1d,e). Since lipophilic dyes, including DiR, may form micelles during labelling, a control experiment was performed in which DiR was added the vehicle (PBS) and prepared and processed in the same manner as DiR labelled EVs. Post ultracentrifugation DiR-Pellets (which would contain any micelles) or DiR-supernatant (Sup) were incubated with HUVECs. While there was very minimal labelling of HUVECs with DiR-Pellet, DiR-Sup containing soluble dye produced a strong DiR signal (Figure S6).

3.2 | Encapsulation of EVs in microgels

Nanoporous hydrogels have been previously used to encapsulate single cells forming a 'microgel' niche to protect cells for in vivo delivery (Kanda et al., 2018). A microfluidic approach (Benavente-Babace et al., 2019; Kanda et al., 2020) was employed to encapsulate EVs labelled with pkh26 in 1% agarose-1% gelatin producing microgels of uniform size ($47 \pm 0.4 \mu$m) (Figure 2a–c). Using confocal imaging z-stacks, labelled EVs were observed to be distributed throughout the spherical microgel, and appeared to be spatially co-localised with the labelled gelatin (Figure 2d). Furthermore, in vitro encapsulated EVs were taken up by both endothelial cells ($9.7 \pm 1\%$) and MØ ($64 \pm 4\%$) over 24 h (Figure 2e,f), and again, uptake of EVs was greater for MØ. Integrated fluorescence density per cell was calculated as a measure of relative EV uptake. Interestingly, there was no difference in the proportion of MØ taking up free versus encapsulated EVs ($p = 0.27$), however, individual MØ took up significantly more free EVs than encapsulated EVs evidenced by higher fluorescent intensity ($p = 0.003$). This demonstrates that microencapsulation delays the uptake of EVs thereby potentially providing a system for controlled delivery of EVs to a target tissue. Interestingly, while the proportion of HUVECs taking up encapsulated EVs was lower than for free EVs, the amount of uptake per cell was if anything higher (Figure 2f), again illustrating important differences in the uptake of EVs between cell types.

3.3 | Microencapsulated EVs enhance local lung specific delivery

To evaluate the impact of encapsulation on EV retention, biodistribution experiments were performed using DiR labelled EVs which has a near-infrared fluorescent signal (ex. 750 nm; em. 780 nm) where tissues have improved optical transparency for in vivo imaging and limited auto-fluorescent. Free or encapsulated EVs and vehicle controls were injected through the jugular vein of SD rats 7 days after administration of MCT (Figure 3a). At 24 h there was a clear difference in biodistribution between free EVs which were predominately taken up by the liver with lung representing only $7.5 \pm 0.4\%$ of the measured fluorescent signal, whereas EV-loaded microgels were efficiently retained within the lung (Figure 3b,c) representing $81 \pm 12\%$ of the signal ($p = 0.0001$). In contrast, EV-loaded microgels show minimal accumulation within the liver at 24 h ($10 \pm 3\%$) compared to $74 \pm 2\%$ for free EVs ($p = 0.0001$). Accumulation of free and encapsulated EVs was not statistically significant in any other organ examined, including spleen, kidney and heart (Figure S7). The fluorescent signal measured in the lungs of encapsulated EVs appeared
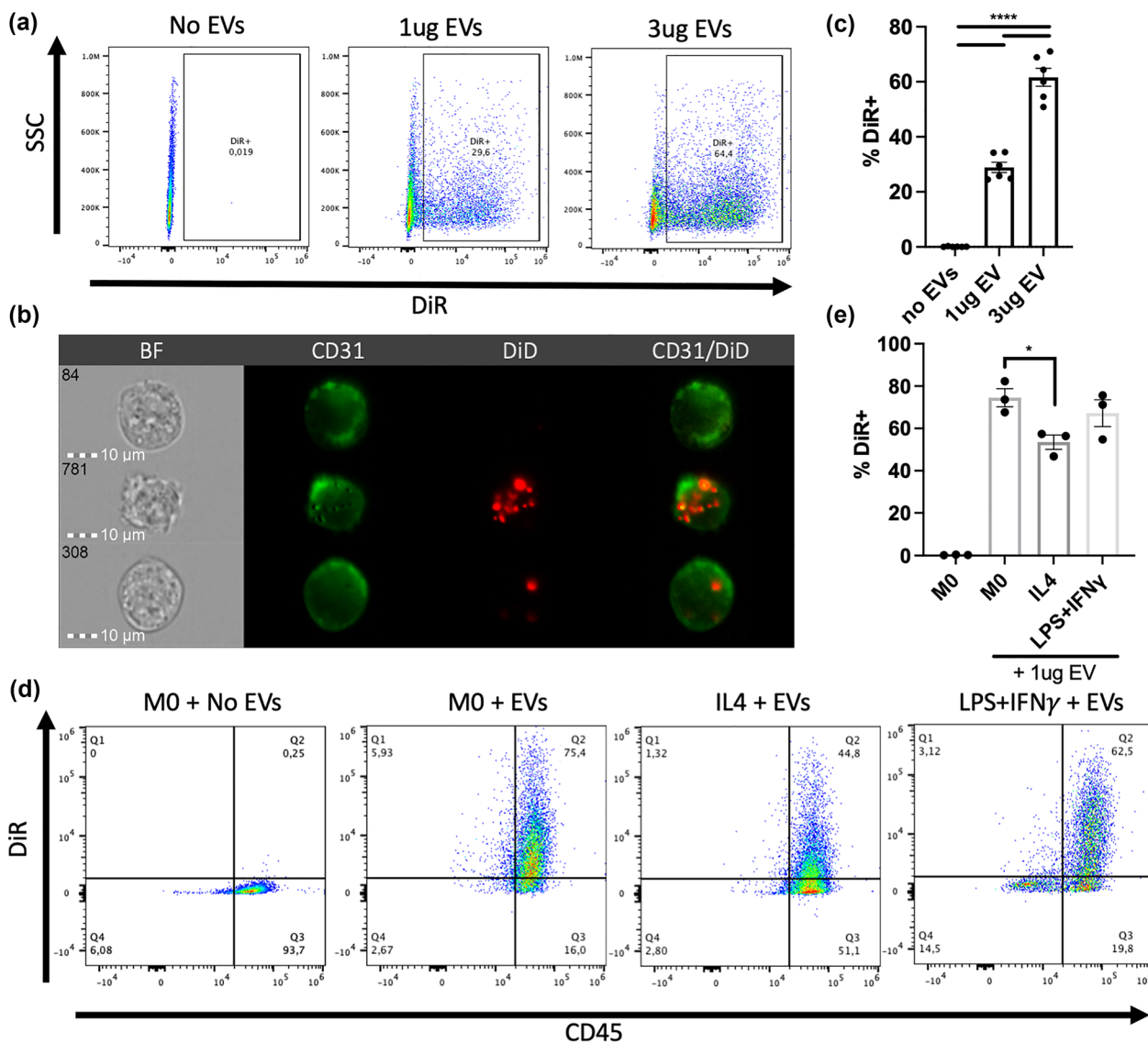
FIGURE 1 Endothelial cells and macrophages have differential MSC-EV uptake. HUVEC and macrophages were exposed to DiR labelled MSC-EVs in vitro. EV uptake by HUVEC was characterised after 24 h by (a) flow cytometry and (b) AMNIS analysis revealing the internalisation of EVs by a limited population of HUVEC, as quantified (c). Unstimulated macrophages (MØ), IL4 stimulated, and LPS+IFNγ stimulated macrophages readily took up EVs as shown in representative flow plots (d) and quantified (e). Data represents mean ± SEM, $n = 3–6$ as indicated by dots.

to increase overtime (Figure 3d,e), which is surprising since the microgels are too large to pass through the pulmonary circulation, and one would anticipate retention at the pre-capillary arteriolar level on first passage. Therefore, the maximal number of encapsulated EVs would be expected immediately after injection. However, the phenomenon of aggregation caused quenching (ACQ) has been well described by Li et al. (2019), resulting in loss of fluorescence signal when fluorescent molecules are densely packed into a restricted space, as with encapsulation. Therefore, it is likely that at early time points the low fluorescent signal was caused by quenching of the fluorescent signal of EVs tightly packed inside microgels (Qi et al., 2019) and that the quenching is reduced as EVs are released over time and become distributed over a greater area. An alternative explanation would be that EVs are taken up over time from the circulation; however, this is unlikely since there was no similar increase in lung signal after the injection of free EVs, which based on their small size would have a much greater opportunity for recirculation. Moreover, vortex-emulsion produced empty 1% agarose-1% gelatin microgels are largely cleared over the first 72 h (Figure S8). While vortex-emulsion microgels were more heterogenous in size, the average diameter was similar ($35 \pm 15\,\mu$m). Finally, it should be noted that the lipophilic dye will persist in the membrane of cells after uptake of EVs and this likely accounts for the relatively stable signal intensity from 4 h to 72 h after delivery of free EVs in the liver, spleen, kidney and heart (Figure S7). Therefore, in aggregate, these findings demonstrate that microencapsulation of small EVs can lead to significant improvement in local lung delivery compared to systemic injection of free EVs.
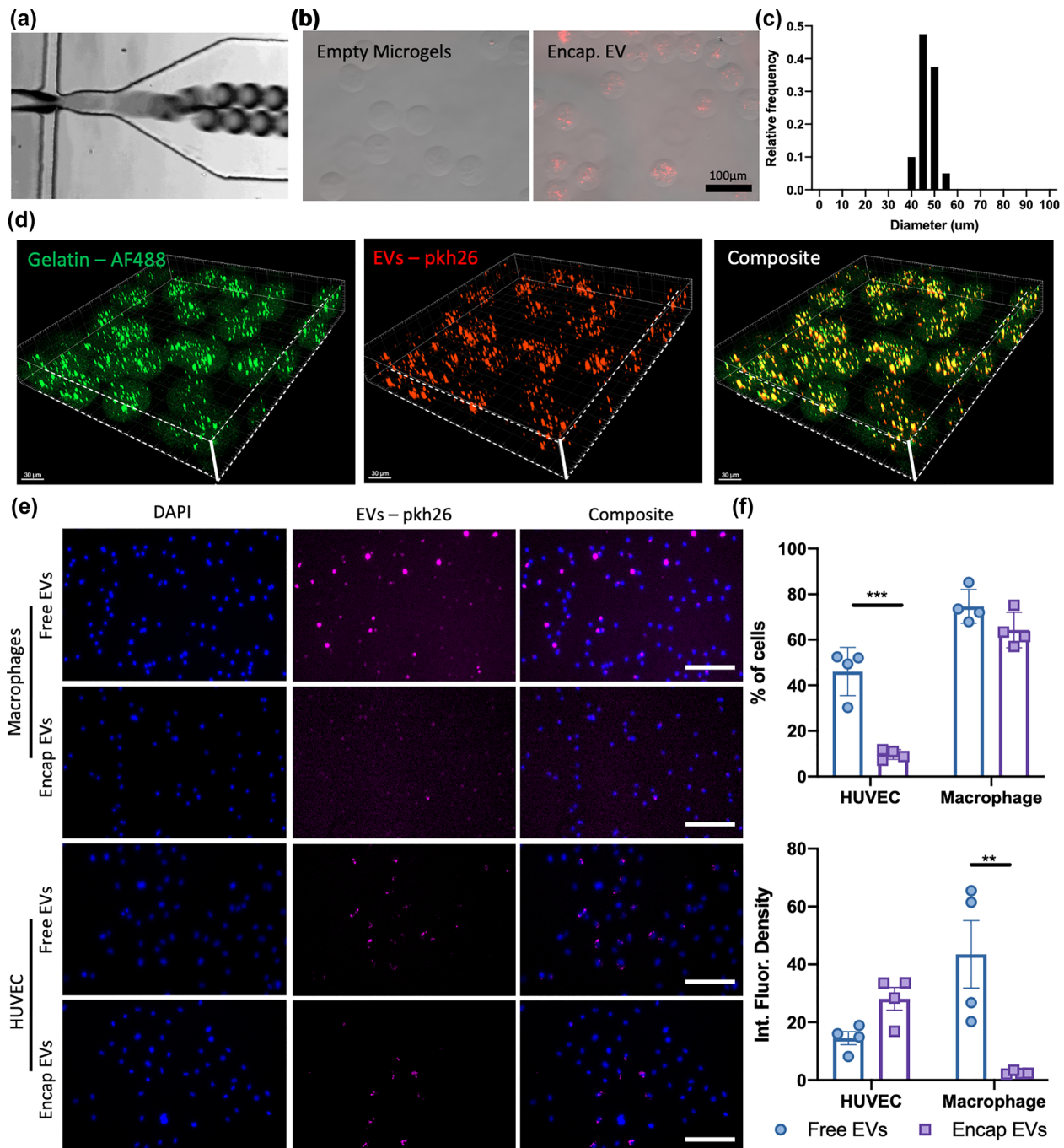
FIGURE 2 Microencapsulation of MSC-EVs within nanoporous hydrogels. (a) Microfluidic encapsulation was performed with 1% agarose-1% gelatin hydrogels using an oil immersion process to form a homogenous population of EV-loaded microgels. Pkh26 labelled encapsulated EVs were visualised by fluorescent microscopy (b) and microgel diameter quantified (c). Confocal z-stacks demonstrate the loading of EVs throughout the hydrogels (d). Uptake of encapsulated EVs was compared to free EVs after 24 h by immunofluorescent imaging (e) and quantification (f) demonstrated the reduced rate of EV uptake compared to free EVs, where scale bar represents 100 μm. Data represents mean $\pm$ SEM, $n = 4$.

3.4 | Encapsulated EVs were taken up by lung resident immune cells in vivo

While the distribution kinetics of free EVs have been studied following systemic administration, little is known about the cellular uptake of these membrane-bound particles in the target organs. We performed lung digestion combined with flow cytometric analysis following the in vivo administration of DiR labelled encapsulated or free EVs to identify which cells were interacting with the administered EVs in the lung. The digestion and isolation procedure was biased towards immune cells, with a large proportion of cells being CD45$^+$ across all treatment groups (Figure 4a,b). Intravenous injection of microgels, with or without, EVs resulted
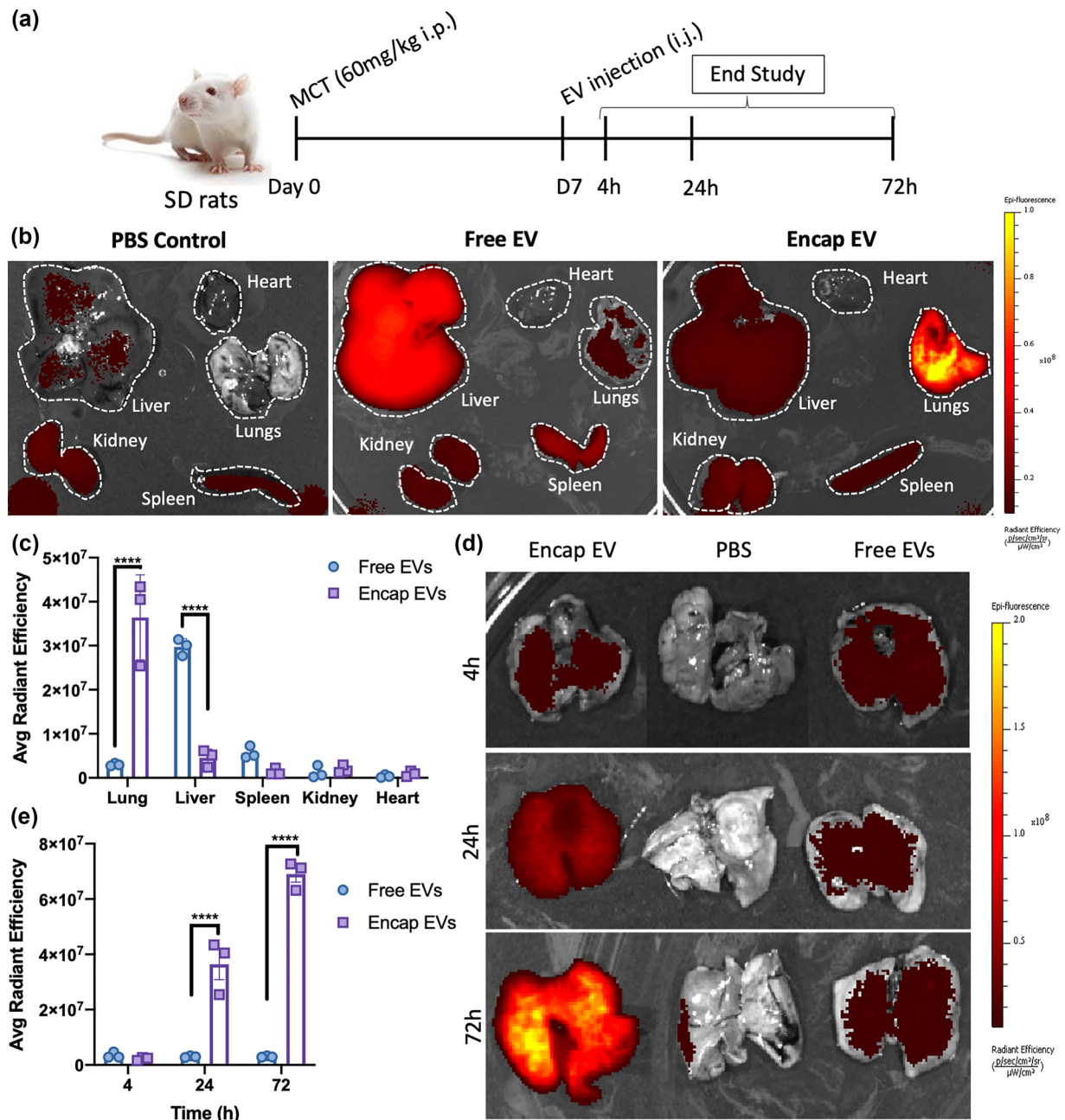
FIGURE 3 EV loaded microgels were retained within the lungs. (a) Free and encapsulated DiR labelled EVs were administered 7 days after monocrotaline (MCT) which induces a model of pulmonary arterial hypertension. (b) Representative images from IVIS analysis demonstrate the level of background fluorescence observed at 24 h in PBS controls compared to free and encapsulated EVs. (c) Quantification of average radiant efficiency at 24 h from the lungs, liver, spleen, kidney and heart demonstrate the significant increase in lung specific retention by encapsulated EVs while free EVs were rapidly cleared to the liver. (d) Representative lung samples from 4 h, 24 h and 72 h time points demonstrate the low level of free EV retention within the lungs, which is further quantified (e). Data represents mean $\pm$ SEM, $n = 3$.

in an increase in CD45$^+$ cell recruitment to the lungs compared to healthy controls (Figure 4b), consistent with a proinflammatory effect of agarose-based hydrogel. Histological data corroborated this finding demonstrating cellular influx surrounding microgels (Figure S8). No statistical difference was observed between the number of endothelial cells (CD45$^-$CD31$^+$) in control lungs and those from animals receiving microgels; while there was a modest increase in other CD45- cells (e.g., fibroblasts) between empty microgels and other groups, consistent with a reactive response (Figure 4b). Interestingly, at 24 h, only animals treated with EV-loaded microgels showed statistically significant accumulation of DiR+ EVs within both the CD45$^+$CD31$^-$ and CD45$^+$CD31lo immune cell populations compared to all other treatment groups (Figure 4c,d). Despite the relative low yield of endothelial cells (CD45$^-$CD31$^+$) from the digestion, EV uptake was seen only in animals receiving EV-loaded microgels. No
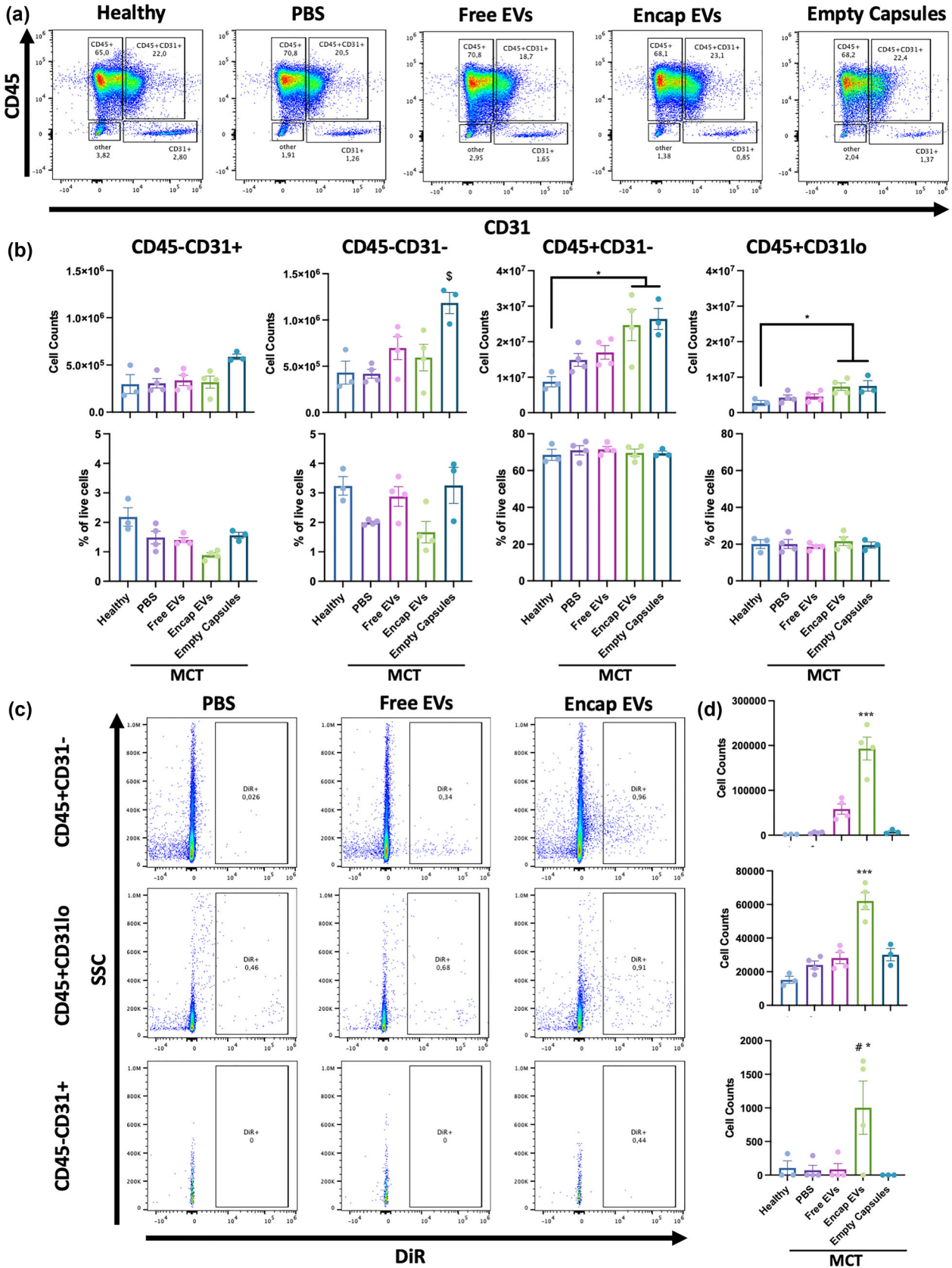
FIGURE 4 Local immune cell EV uptake increased by microencapsulation. Lungs were isolated, digested and prepared for flow cytometry analysis 24 h after DiR labelled EV administration. (a) Representative flow plots demonstrate consistent proportions of lung endothelial (CD45$^-$CD31$^+$), immune (CD45$^+$CD31$^-$ or CD31lo), and other (CD45$^-$CD31$^-$) populations, which was quantified as cell counts, and proportions (b) demonstrating increased numbers

(Continues)

FIGURE 4 (Continued)

of immune cells with the presence of microgels. EV uptake was assessed by evaluation of DiR labelling, representative flow plots are shown (c) and quantification (d) demonstrates significant EV uptake by CD45$^+$CD31$^-$ and CD45$^+$ CD31lo cells when exposed to encapsulated EVs. Data represented as mean ± SEM, n = 3–4; $ $p < 0.05$ healthy, PBS and Encap EVs compared to Empty Capsules; *$p < 0.05$ PBS, Free EVs and Empty Capsules compared to Encap. EVs; ***$p < 0.0005$ all Tx compared to Encap EVs; #$p = 0.07$ healthy compared to Encap EVs.

differences were observed in the CD45$^-$CD31$^-$ cells uptake of DiR+ EVs between all the treatment groups (Figure S9). Therefore, these findings demonstrate that EVs are predominately taken up by immune cells in vivo, and encapsulation enhances EV uptake.

4 | DISCUSSION

Systemic delivery of free EVs is a promising treatment for a variety of lung diseases (Mohan et al., 2020), including PAH (Klinger et al., 2019). However, after intravenous administration, EVs are rapidly cleared from the circulation, primarily by the liver and spleen (Abello et al., 2019; Gupta et al., 2020; Kang et al., 2021; Wiklander et al., 2015), representing a significant challenge for therapies requiring targeted delivery of EVs to other tissues and organs, such as the lungs. Therefore, strategies to improve organ-specific EV retention and prolong the opportunity for EVs to interact with target host cells could greatly enhance the efficacy of EV therapies. In this study, we demonstrated that encapsulation of MSC-EVs in nano-porous microgels significantly improved lung targeted EV retention and enhanced EV uptake by resident lung cells.

Microencapsulation has been previously employed for the delivery of therapeutic stem and progenitor cells (Kanda et al., 2018, 2020; Karoubi et al., 2009). We sought to apply this technology for the targeted delivery of EVs to the lung. We demonstrated reduced uptake of EVs in vitro over 24 h by macrophages (decreased EV fluorescent signal) and ECs (decreased percentage of EV+ cells) from microgels suggesting that encapsulation restricted access to EVs compared to free EVs which were readily taken up by cells. The marked difference in the way ECs and macrophages interacted with encapsulated EVs suggests cell type has an important impact on EV uptake. Phagocytic cells, such as macrophages, show greater consistency of EV uptake than ECs; however, the magnitude of EV uptake was greatly constrained by encapsulation. In contrast, a smaller proportion of ECs were able to uptake EVs, especially after encapsulation, but the number of EVs taken up remained fairly constant. We cannot rule out that other factors, including differences in cell culture media and additives, might influence EV release from the microgels and cellular uptake. Despite the relatively restricted uptake of encapsulated EVs over 24 h in cell culture conditions, in vivo studies demonstrated much greater retention of EV containing microgels within the lungs up to 72 h following injection. This is in contrast to previous pharmacokinetic studies which have shown that free EVs are rapidly cleared from the bloodstream within hours of administration (Gupta et al., 2020). Therefore, loading EVs into microgels represents an effective strategy to both enhance their delivery to the lung and increase their retention.

While previous studies have evaluated the overall biodistribution of systemically administered EVs, they have generally not examined which cells are responsible for EV uptake. To better understand the mechanisms by which EVs may exert their therapeutic actions, it is necessary to define the specific cell types with which they interact. In this study, we used fluorescently labelled EVs in combination with lung digestion and flow cytometry to gain insights into the cellular uptake of MSC-EVs within the lung. Loading EVs into microgels resulted in a marked increase in uptake by lung resident cells, primarily CD45$^+$ immune cells. Uptake by lung resident immune cells could enhance the therapeutic efficacy of EVs in inflammatory lung diseases, such as acute respiratory distress syndrome. As well, in PAH it is hypothesized that MSC-derived EVs modulate the local inflammatory environment by interacting with immune cells, specifically macrophages (Willis et al., 2018). While free EVs were readily taken up by macrophages in vitro (Figure 1), due to the short residence time in vivo, their ability to interact with lung host cells was limited resulting in minimal uptake by CD45$^+$ immune cells after systemic delivery (Figure 4). In contrast, microencapsulation, which reduced in vitro uptake by MØ and ECs, greatly enhanced cellular uptake in vivo by prolonging the retention of EV-loaded microgels in the lung. However, whether the more efficient lung resident cell uptake of encapsulated EVs translates into greater therapeutic benefits remains to be seen.

The biomaterials used for microgel preparation will impact the tissue residence time and the local microenvironment. An agarose hydrogel formulation was developed for previous studies in our group designed to enhance cell persistence and engraftment following transplantation (Karoubi et al., 2009). This agarose-gelatin formulation was also effective in enhancing local retention of encapsulated EVs in the lung (Figure 3), yet there are opportunities to optimise the biomaterial formulation going forward. Interestingly, fluorescently labelled gelatin and EVs appeared to co-localise within microgels (Figure 2), which may be due to protein-protein interactions between the gelatin and EVs during microgel formation and could contribute to the EV protein corona. While modifications to the EV protein corona were not directly studied, changes to the protein corona could influence downstream EV-cell interactions (Wolf et al., 2022), and the impact of microgel encapsulation on this could be the

source of future studies. Immune cells were the primary cells involved in the uptake of EVs from microgels and even empty agarose-gelatin microgels promoted inflammation, as observed by increased number of immune cells within the lung, likely due to biomaterial-immune cell interactions inciting a local foreign body response (FBR). The size and shape of implanted biomaterials has been shown to influence the FBR, although in this study no materials below 100 μm were studied (Veiseh et al., 2015).

Novel biomaterials have been developed to reduce the FBR, for example to reduce the inflammatory response to encapsulated pancreatic islets after transplantation (Vegas et al., 2016). Further studies should seek to optimise the biomaterial formulation to reduce the FBR, particularly in the context of a therapeutic product. Biomaterials can also be modified to optimise the release kinetics of EVs. Recently, it has been reported that translocation of EVs through biomaterials and extracellular matrices is linked to the matrix mechanical properties and the EV deformability (Lenzini et al., 2020), and this represents an opportunity to modify the matrix properties to control the diffusivity of the loaded EVs. Alternatively, introduction of matrix metalloproteinase degradable sites through click-chemistries (Tam et al., 2017) could further refine the release profile and determine the local retention time by enhancing degradation of the microgels.

This study demonstrates that EV-loaded microgels can be used to enhance EV delivery to the lungs compared to administration of free EVs. Furthermore, EV-loaded microgels act as a sustained release system to increase the time for interaction between host cells and EVs. Lastly, we have demonstrated that increased local retention of EVs results in significantly higher host cell uptake. All of this suggests EV-loaded microgels may offer significant benefits to enhancing the delivery of EV therapies.

AUTHOR CONTRIBUTIONS
Nicholas D. Cober: Conceptualization; Data curation; Formal analysis; Investigation; Methodology; Project administration; Validation; Visualization; Writing – original draft; Writing – review & editing. **Katelynn Rowe**: Conceptualization; Investigation; Methodology; Visualization. **Yupu Deng**: Investigation; Methodology. **Ainara Benavente-Babace**: Investigation; Methodology; Resources. **David W. Courtman**: Methodology; Supervision; Writing – review & editing. **Michel Godin**: Methodology; Resources; Writing – review & editing. **Duncan J. Stewart**: Conceptualization; Formal analysis; Funding acquisition; Methodology; Project administration; Resources; Supervision; Validation; Visualization; Writing – original draft; Writing – review & editing.

CONFLICT OF INTEREST STATEMENT
The authors declare no conflicts of interest.

DATA AVAILABILITY STATEMENT
The data that support the findings of this study are available from the corresponding author upon reasonable request.

ORCID
Nicholas D. Cober https://orcid.org/0000-0001-8061-806X
David W. Courtman https://orcid.org/0000-0002-6403-271X
Michel Godin https://orcid.org/0000-0002-9360-0675
Duncan J. Stewart https://orcid.org/0000-0002-9113-8691

REFERENCES
Abello, J., Nguyen, T. D. T., Marasini, R., Aryal, S., & Weiss, M. L. (2019). Biodistribution of gadolinium- and near infrared-labeled human umbilical cord mesenchymal stromal cell-derived exosomes in tumor bearing mice. *Theranostics*, *9*, 2325.

Benavente-Babace, A., Haase, K., Stewart, D. J., & Godin, M. (2019). Strategies for controlling egress of therapeutic cells from hydrogel microcapsules. *Journal of Tissue Engineering and Regenerative Medicine*, *13*, 612–624.

Bian, S., Zhang, L., Duan, L., Wang, X., Min, Y., & Yu, H. (2014). Extracellular vesicles derived from human bone marrow mesenchymal stem cells promote angiogenesis in a rat myocardial infarction model. *Journal of Molecular Medicine*, *92*, 387–397.

Colombo, M., Raposo, G., & Théry, C. (2014). Biogenesis, secretion, and intercellular interactions of exosomes and other extracellular vesicles. *Annual Review of Cell and Developmental Biology*, *30*, 255–289.

Cruz, F. F., & Rocco, P. R. M. (2017). Stem-cell extracellular vesicles and lung repair. *Stem Cell Investigation*, *4*, 78.

de Mendonça, L., Felix, N. S., Blanco, N. G., Da Silva, J. S., Ferreira, T. P., Abreu, S. C., Cruz, F. F., Rocha, N., Silva, P. M., Martins, V., Capelozzi, V. L., Zapata-Sudo, G., Rocco, P. R. M., & Silva, P. L. (2017). Mesenchymal stromal cell therapy reduces lung inflammation and vascular remodeling and improves hemodynamics in experimental pulmonary arterial hypertension. *Stem Cell Research & Therapy*, 8, 220.

Godoy, R. S., Cober, N., Cook, D. P., McCourt, E., Deng, Y., Wang, L., Schlosser, K., Rowe, K., & Stewart, D. J. (2023). Single cell transcriptomic atlas of lung microvascaular regeneration after targeted endothelial abalation. *eLife*, 2023, https://doi.org/10.7554/eLife.80900

Gupta, D., Liang, X., Pavlova, S., Wiklander, O. P. B., Corso, G., Zhao, Y., Saher, O., Bost, J., Zickler, A. M., Piffko, A., Maire, C. L., Ricklefs, F. L., Gustafsson, O., Llorente, V. C., Gustafsson, M. O., Bostancioglu, R. B., Mamand, D. R., Hagey, D. W., Görgens, A., … El Andaloussi, S. (2020). Quantification of extracellular vesicles in vitro and in vivo using sensitive bioluminescence imaging. *Journal of Extracellular Vesicles*, 9(1), 1800222. https://doi.org/10.1080/20013078.2020.1800222

Hurskainen, M., Mižíková, I., Cook, D. P., Andersson, N., Cyr-Depauw, C., Lesage, F., Helle, E., Renesme, L., Jankov, R. P., Heikinheimo, M., Vanderhyden, B. C., & Thébaud, B. (2021). Single cell transcriptomic analysis of murine lung development on hyperoxia-induced damage. *Nature Communications*, 12(1), 1–19.

Kanda, P., Alarcon, E. I., Yeuchyk, T., Parent, S., de Kemp, R. A., Variola, F., Courtman, D., Stewart, D. J., & Davis, D. R. (2018). Deterministic encapsulation of human cardiac stem cells in variable composition nanoporous gel cocoons to enhance therapeutic repair of injured myocardium. *ACS Nano*, 7b08881. https://doi.org/10.1021/acsnano.7b08881

Kanda, P., Benavente-Babace, A., Parent, S., Connor, M., Soucy, N., Steeves, A., Lu, A., Cober, N. D., Courtman, D., Variola, F., Alarcon, E. I., Liang, W., Stewart, D. J., Godin, M., & Davis, D. R. (2020). Deterministic paracrine repair of injured myocardium using microfluidic-based cocooning of heart explant-derived cells. *Biomaterials*, 247, 120010. https://doi.org/10.1016/j.biomaterials.2020.120010

Kang, M., Jordan, V., Blenkiron, C., & Chamley, L. W. (2021). Biodistribution of extracellular vesicles following administration into animals: A systematic review. *Journal of Extracellular Vesicles*, 10(8), e12085. Preprint at https://doi.org/10.1002/jev2.12085

Karoubi, G., Ormiston, M. L., Stewart, D. J., & Courtman, D. W. (2009). Single-cell hydrogel encapsulation for enhanced survival of human marrow stromal cells. *Biomaterials*, 30, 5445–5455.

Klinger, J. R., Pereira, M., Del Tatto, M., Brodsky, A. S., Wu, K. Q., Dooner, M. S., Borgovan, T., Wen, S., Goldberg, L. R., Aliotta, J. M., Ventetuolo, C. E., Quesenberry, P. J., & Liang, O. D. (2019). Mesenchymal stem cell extracellular vesicles reverse sugen/hypoxia pulmonary hypertension in rats. *American Journal of Respiratory Cell and Molecular Biology*, https://doi.org/10.1165/rcmb.2019-0154oc

Kou, M., Huang, L., Yang, J., Chiang, Z., Chen, S., Liu, J., Guo, L., Zhang, X., Zhou, X., Xu, X., Yan, X., Wang, Y., Zhang, J., Xu, A., Tse, H. F., & Lian, Q. (2022). Mesenchymal stem cell-derived extracellular vesicles for immunomodulation and regeneration: A next generation therapeutic tool? *Cell Death & Disease*, 13(7), 1–16.

Lai, C. P., Mardini, O., Ericsson, M., Prabhakar, S., Maguire, C., Chen, J. W., Tannous, B. A., & Breakefield, X. O. (2014). Dynamic biodistribution of extracellular vesicles in vivo using a multimodal imaging reporter. *ACS Nano*, 8, 483–494.

Lenzini, S., Bargi, R., Chung, G., & Shin, J. W. (2020). Matrix mechanics and water permeation regulate extracellular vesicle transport. *Nature Nanotechnology*, 15, 217–223.

Li, Y., Wu, Y., Chen, J., Wan, J., Xiao, C., Guan, J., Song, X., Li, S., Zhang, M., Cui, H., Li, T., Yang, X., Li, Z., & Yang, X. (2019). A simple glutathione-responsive turn-on theranostic nanoparticle for dual-modal imaging and chemo-photothermal combination therapy. *Nano Letters*, 19, 5806–5817.

Lv, K., Li, Q., Zhang, L., Wang, Y., Zhong, Z., Zhao, J., Lin, X., Wang, J., Zhu, K., Xiao, C., Ke, C., Zhong, S., Wu, X., Chen, J., Yu, H., Zhu, W., Li, X., Wang, B., Tang, R., … Hu, X. (2019). Incorporation of small extracellular vesicles in sodium alginate hydrogel as a novel therapeutic strategy for myocardial infarction. *Theranostics*, 9, 7403–7416.

Mohan, A., Agarwal, S., Clauss, M., Britt, N. S., & Dhillon, N. K. (2020). Extracellular vesicles: Novel communicators in lung diseases. *Respiratory Research*, 21, 1–21. Preprint at https://doi.org/10.1186/s12931-020-01423-y

Porzionato, A., Zaramella, P., Dedja, A., Guidolin, D., Bonadies, L., Macchi, V., Pozzobon, M., Jurga, M., Perilongo, G., De Caro, R., Baraldi, E., & Muraca, M. (2021). Intratracheal administration of mesenchymal stem cell-derived extracellular vesicles reduces lung injuries in a chronic rat model of bronchopulmonary dysplasia. *American Journal of Physiology-Lung Cellular and Molecular Physiology*, 320(5), L688–L704. https://doi.org/10.1152/ajplung.00148.2020

Qi, J., Hu, X., Dong, X., Lu, Y., Lu, H., Zhao, W., & Wu, W. (2019). Towards more accurate bioimaging of drug nanocarriers: Turning aggregation-caused quenching into a useful tool. *Advanced Drug Delivery Reviews*, 143, 206–225.

Royo, F., Cossío, U., Ruiz De Angulo, A., Llop, J., & Falcon-Perez, J. M. (2019). Modification of the glycosylation of extracellular vesicles alters their biodistribution in mice. *Nanoscale*, 11, 1531–1537.

Song, K., Huang, M., Shi, Q., Du, T., & Cao, Y. (2014). Cultivation and identification of rat bone marrow-derived mesenchymal stem cells. *Molecular Medicine Reports*, 10, 755–760.

Souza-Moreira, L., Soares, V. C., Dias, S., da, S. G., & Bozza, P. T. (2019). Adipose-derived mesenchymal stromal cells modulate lipid metabolism and lipid droplet biogenesis via AKT/mTOR –PPARγ signalling in macrophages. *Scientific Reports*, 9(1), 20304.

Tam, R. Y., Smith, L. J., & Shoichet, M. S. (2017). Engineering cellular microenvironments with photo- and enzymatically responsive hydrogels: Toward biomimetic 3D cell culture models. *Accounts of Chemical Research*, 50, 703–713.

Théry, C., Witwer, K. W., Aikawa, E., Alcaraz, M. J., Anderson, J. D., Andriantsitohaina, R., Antoniou, A., Arab, T., Archer, F., Atkin-Smith, G. K., Ayre, D. C., Bach, J. M., Bachurski, D., Baharvand, H., Balaj, L., Baldacchino, S., Bauer, N. N., Baxter, A. A., Bebawy, M., … Zuba-Surma, E. K. (2018). Minimal information for studies of extracellular vesicles 2018 (MISEV2018): A position statement of the International Society for Extracellular Vesicles and update of the MISEV2014 guidelines. *Journal of Extracellular Vesicles*, 7, 1535750.

Thomas, D., O'Brien, T., & Pandit, A. (2018). Toward customized extracellular niche engineering: Progress in cell-entrapment technologies. *Advanced Materials*, 30, 1703948.

Tieu, A., Stewart, D. J., & Lalu, M. M. (2020). Mesenchymal stem cell-derived extracellular vesicles: Good things come in small packages. *Critical Care Medicine*, 48, 1095–1097. Preprint at https://doi.org/10.1097/CCM.0000000000004368

Vegas, A. J., Veiseh, O., Doloff, J. C., Ma, M., Tam, H. H., Bratlie, K., Li, J., Bader, A. R., Langan, E., Olejnik, K., Fenton, P., Kang, J. W., Hollister-Locke, J., Bochenek, M. A., Chiu, A., Siebert, S., Tang, K., Jhunjhunwala, S., Aresta-Dasilva, S., … Anderson, D. G. (2016). Combinatorial hydrogel library enables identification of materials that mitigate the foreign body response in primates. *Nature Biotechnology*, 34, 345–352.

Veiseh, O., Doloff, J. C., Ma, M., Vegas, A. J., Tam, H. H., Bader, A. R., Li, J., Langan, E., Wyckoff, J., Loo, W. S., Jhunjhunwala, S., Chiu, A., Siebert, S., Tang, K., Hollister-Lock, J., Aresta-Dasilva, S., Bochenek, M., Mendoza-Elias, J., Wang, Y., … Anderson, D. G. (2015). Size- and shape-dependent foreign body immune response to materials implanted in rodents and non-human primates. *Nature Materials*, 14, 643–651.

Wang, J., Huang, R., Xu, Q., Zheng, G., Qiu, G., Ge, M., Shu, Q., & Xu, J. (2020). Mesenchymal stem cell-derived extracellular vesicles alleviate acute lung injury via transfer of miR-27a-3p. *Critical Care Medicine*, 48, E599–E610.

Wang, N., Chen, C., Yang, D., Liao, Q., Luo, H., Wang, X., Zhou, F., Yang, X., Yang, J., Zeng, C., & Wang, W. E. (2017). Mesenchymal stem cells-derived extracellular vesicles, via miR-210, improve infarcted cardiac function by promotion of angiogenesis. *Biochimica et Biophysica Acta (BBA) - Molecular Basis of Disease*, *1863*, 2085–2092.

Wen, S. W., Sceneay, J., Lima, L. G., Wong, C. S., Becker, M., Krumeich, S., Lobb, R. J., Castillo, V., Wong, K. N., Ellis, S., Parker, B. S., & Möller, A. (2016). The biodistribution and immune suppressive effects of breast cancer-derived exosomes. *Cancer Research*, *76*, 6816–6827.

Wen, S. W., Sceneay, J., Lima, L. G., Wong, C. S., Becker, M., Krumeich, S., Lobb, R. J., Castillo, V., Wong, K. N., Ellis, S., Parker, B. S., & Möller, A. (2021). Selection of fluorescent, bioluminescent, and radioactive tracers to accurately reflect extracellular vesicle biodistribution in vivo. *ACS Nano*, *15*, 3212–3227.

Wiklander, O. P., Nordin, J. Z., O'Loughlin, A., Gustafsson, Y., Corso, G., Mäger, I., Vader, P., Lee, Y., Sork, H., Seow, Y., Heldring, N., Alvarez-Erviti, L., Smith, C. I., Le Blanc, K., Macchiarini, P., Jungebluth, P., Wood, M. J., & Andaloussi, S. E. (2015). Extracellular vesicle in vivo biodistribution is determined by cell source, route of administration and targeting. *Journal of Extracellular Vesicles*, *4*, 26316.

Wiklander, O. P., Nordin, J. Z., O'Loughlin, A., Gustafsson, Y., Corso, G., Mäger, I., Vader, P., Lee, Y., Sork, H., Seow, Y., Heldring, N., Alvarez-Erviti, L., Smith, C. I., Le Blanc, K., Macchiarini, P., Jungebluth, P., Wood, M. J., & Andaloussi, S. E. (2015). Extracellular vesicle in vivo biodistribution is determined by cell source, route of administration and targeting. *Journal of Extracellular Vesicles*, *4*, 1–13.

Willis, G. R., Fernandez-Gonzalez, A., Reis, M., Mitsialis, S. A., & Kourembanas, S. (2018). Macrophage immunomodulation: The gatekeeper for mesenchymal stem cell derived-exosomes in pulmonary arterial hypertension? *International Journal of Molecular Sciences*, *19*, 2534.

Wilson, J. G., Liu, K. D., Zhuo, H., Caballero, L., McMillan, M., Fang, X., Cosgrove, K., Vojnik, R., Calfee, C. S., Lee, J. W., Rogers, A. J., Levitt, J., Wiener-Kronish, J., Bajwa, E. K., Leavitt, A., McKenna, D., Thompson, B. T., & Matthay, M. A. (2015). Mesenchymal stem (Stromal) cells for treatment of ARDS: A Phase 1 clinical trial. *The Lancet Respiratory Medicine*, *3*, 24.

Wolf, M., Poupardin, R. W., Ebner-Peking, P., Andrade, A. C., Blöchl, C., Obermayer, A., Gomes, F. G., Vari, B., Maeding, N., Eminger, E., Binder, H. M., Raninger, A. M., Hochmann, S., Brachtl, G., Spittler, A., Heuser, T., Ofir, R., Huber, C. G., Aberman, Z., … Strunk, D. (2022). A functional corona around extracellular vesicles enhances angiogenesis, skin regeneration and immunomodulation. *Journal of Extracellular Vesicles*, *11*(4), e12207.

Xu, J. H., Liang, J. P., Zhu, C. J., & Lian, Y. J. (2022). Mesenchymal stem cell-derived extracellular vesicles therapy for pulmonary hypertension: A comprehensive review of preclinical studies. *Journal of Interventional Cardiology*, *2022*, 5451947.

Yuana, Y., Böing, A. N., Grootemaat, A. E., van der Pol, E., Hau, C. M., Cizmar, P., Buhr, E., Sturk, A., & Nieuwland, R. (2015). Handling and storage of human body fluids for analysis of extracellular vesicles. *Journal of Extracellular Vesicles*, *4*, 29260.

Zhao, Y. D., Courtman, D. W., Deng, Y., Kugathasan, L., Zhang, Q., & Stewart, D. J. (2005). Rescue of monocrotaline-induced pulmonary arterial hypertension using bone marrow-derived endothelial-like progenitor cells: Efficacy of combined cell and eNOS gene therapy in established disease. *Circulation Research*, *96*, 442–450.

SUPPORTING INFORMATION

Additional supporting information can be found online in the Supporting Information section at the end of this article.